JOC The Journal of Organic Chemistry

Article

pubs.acs.org/joc

Anthraphane: An Anthracene-Based, Propeller-Shaped D_{3h}-Symmetric Hydrocarbon Cyclophane and Its Layered Single Crystal Structures

Marco Servalli,*[,†] Nils Trapp,[‡] Michael Wörle,[‡] and Frank-Gerrit Klärner[§]

[†]Laboratory of Polymer Chemistry, Department of Materials, ETH Zurich, Vladimir-Prelog-Weg 5, 8093 Zurich, Switzerland

[‡]Laboratory of Inorganic Chemistry, Small Molecule Crystallography Center, Department of Chemistry and Applied Biosciences, ETH Zurich, Vladimir-Prelog-Weg 1, 8093 Zurich, Switzerland

[§]Institut für Organische Chemie, Universität Duisburg-Essen, Universitätsstrasse 5, 45117 Essen, Germany

Supporting Information

ABSTRACT: The novel hydrocarbon propeller-shaped D_{3h}-symmetric cyclophane (**3**), "anthraphane", was prepared through a revisited and optimized gram-scale synthesis of the key building block anthracene-1,8-ditriflate **7**. Anthraphane has a high tendency to crystallize and single crystals in size ranges of 100−200 μm are easily obtained from different solvents. The crystallization behavior of **3** was extensively studied to unravel packing motifs and determine whether the packing can be steered into a desired direction, so to allow topochemical photopolymerization. SC-XRD shows that anthraphane packs in layers irrespective of the solvent used for crystallization. However, within the layers, intermolecular arrangements and $\pi-\pi$ interactions of the anthracene units vary strongly. Four interaction motifs for the anthracene moieties are observed and discussed in detail: two types of exclusively edge-to-face (*etf*), a mixture of edge-to-face and face-to-face (*ftf*), and no anthracene−anthracene interaction at all. To elucidate why an exclusive *ftf* stacking was not observed, electrostatic potential surface (EPS) calculations with the semiempirical PM3 method were performed. They show qualitatively that the anthracene faces bear a strong negative surface potential, which may be the cause for this cyclophane to avoid *ftf* interactions. This combined crystallographic and computational study provides valuable insights on how to create all-*ftf* packings.

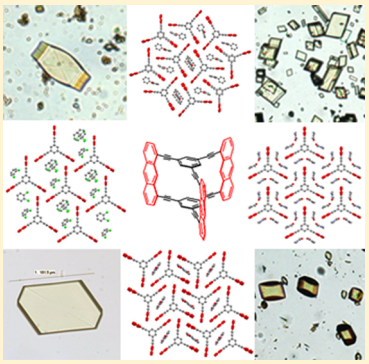

INTRODUCTION

Two-dimensional polymers[1,2] and related covalent monolayer sheets[3−5] have recently been synthesized by exploiting controlled photoinduced growth in two-dimensionally confined dimensions, either topochemically in layered single crystals[6−9] or at the air/water interface.[10] This successful synthetic strategy requires the monomers to have at least three photoreactive units embedded in the proper geometry, allowing a two-dimensional growth, in this case brought about by the well-studied photoinduced dimerization of anthracenes via [4 + 4]-cycloaddition.[11,12]

Monomers **1** and **2** are prominent examples (Figure 1). For the polymerization to take place, the anthracene moieties have to be in close contact (typically at or below the Schmidt distance of 4.2 Å[13]) in a face-to-face (*ftf*) $\pi-\pi$ stacked arrangement. While there are several factors influencing the packing of organic compounds in a crystal,[14,15] the success with monomers **1** and **2** suggests that their structures consisting of three anthracene blades embedded in a 3-fold symmetric, shape-persistent arrangement seems to be helpful in attaining a packing for lateral polymerization. We therefore started exploring for new compounds meeting the same criteria and report here on the synthesis of cyclophane (**3**). Due to its structural features, the compound was conveniently named "anthraphane": a portmanteau word of "anthracene" and "cyclophane". This novel hydrocarbon[16] can be obtained on a 100 mg scale in only five steps from commercial starting materials, and for its preparation, it was instrumental to revisit and improve the known synthesis of a key intermediate, anthracene-1,8-ditriflate **7**.

Furthermore, we present several single-crystal X-ray diffraction (SC-XRD) structures of crystals grown from **3** and discuss the various structural motifs obtained from the 14 different solvents used. Finally, strategies will be assessed to eventually obtain a packing in which all anthracene units are *ftf* stacked relative to one another, which is the key arrangement for lateral polymerization. This discussion is supported by semiempirical PM3 calculations, which show that the electrostatic potential surface (EPS) of the anthracene units is strongly negatively charged. This effect needs to be counteracted to allow *ftf* interactions. However, *ftf* or at least displaced *ftf* orientations of two benzene, naphthalene, or anthracene rings have been calculated using high-level quantum chemical methods to be stable too, whereas in the crystalline state the aromatic systems often prefer *etf* orientations.[17−19]

Received: January 29, 2016
Published: February 26, 2016

DOI: 10.1021/acs.joc.6b00209
J. Org. Chem. 2016, 81, 2572−2580

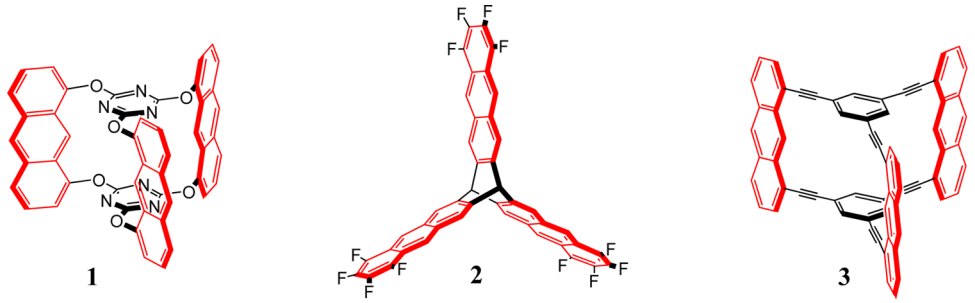

Figure 1. Chemical structures of monomers **1** and **2** and anthraphane (**3**) presented in this study. All have a propeller geometry with three anthracene blades embedded in a 3-fold symmetry (**1**, **3**, 1,8-anthryl; **2**, 2,3-anthryl).

Scheme 1. (a) Synthetic Route for the Novel Synthesis of Key Building Block 7. (b) Sequential Sonogashira Cross-Coupling Reactions of 7 and 1,3,5-Triethynylbenzene (8) To Yield Anthraphane (3)[a]

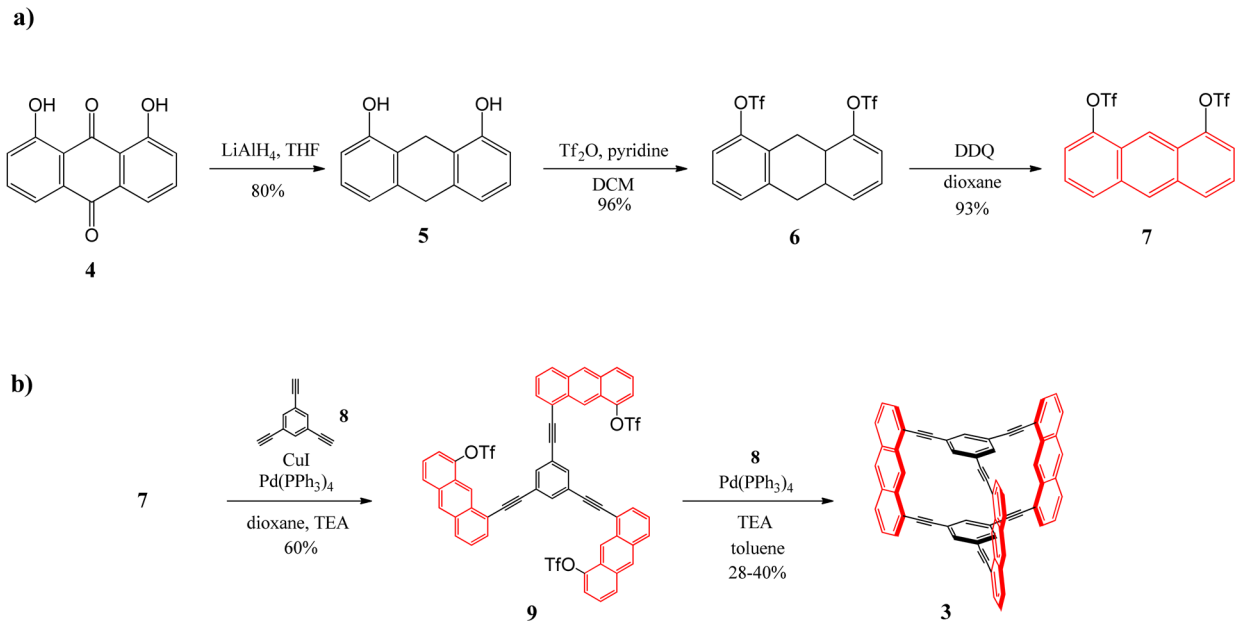

[a]Despite the complexity of the final step, a difficult sequence of intermolecular and intramolecular couplings, surprisingly high yields ranging from 28 to 40% were obtained.

RESULTS AND DISCUSSION

Synthesis of Anthraphane. The novel, five-step synthetic route to anthraphane (**3**) is depicted in Scheme 1. As a coupling partner for the Sonogashira reaction with the commercially available 1,3,5-triethynylbenzene (**8**), we wanted to use a building block that could be easily synthesized in gram scale and with little effort. The natural choice of using the halogenated 1,8-dibromoanthracene[20] or 1,8-diiodoanthracene[21] was discarded as their synthesis, starting from 1,8-dichloroanthraquinone, involves refluxing toxic nitrobenzene for the halogen-exchange reaction followed by two sequential reductions of the anthrone moieties with sodium borohydride proceeding with moderate yields. We therefore concentrated our effort on the anthracene-1,8-ditriflate **7**, as the triflate groups are generally introduced with high yields and confer solubility, and their reactivity toward oxidative addition lies between that of bromide and iodide.[22] However, this required the existing synthesis of **7** to be substantially improved.[23] The previously known route passes through a couple of tedious and time-consuming steps which render the synthesis a demanding procedure (for details, see Scheme S1 in the Supporting Information).

We therefore devised a new route (Scheme 1a) which provides this desired intermediate with a total yield of up to 71% (previously: 27%) on a 15 g scale and within 1 week.

The new route starts from 1,8-dihydroxyanthraquinone **4**, whose lithium aluminum hydride reduction leading to the stable 1,8-dihydroxy-9,10-dihydroanthracene **5** had already been reported.[24] By applying standard triflation conditions to **5** with triflic anhydride and pyridine in dichloromethane, the ditriflated compound **6** can be smoothly obtained in virtually quantitative yield on a 15 g scale within a 2 h time. Purification involves standard workup followed by treatment of the crude product with activated charcoal in boiling hexane and hot filtration over Celite. This triflation step is an asset of the whole procedure as it is performed on **5**, which is a phenol derivative and thus not sensitive under the basic conditions required for triflation, unlike the 1,8-dihydroxyanthracene used in the traditional synthesis. In the final step, aromatization to the target compound **7** is achieved in yields up to 93% by refluxing **6** with DDQ in dry dioxane for 5 h. Simple filtration over a silica plug affords the pure product, whose elution can be followed conveniently under UV light. *p*-Chloranil was also tested as an aromatization reagent but found to be less effective

DOI: 10.1021/acs.joc.6b00209
J. Org. Chem. 2016, 81, 2572−2580

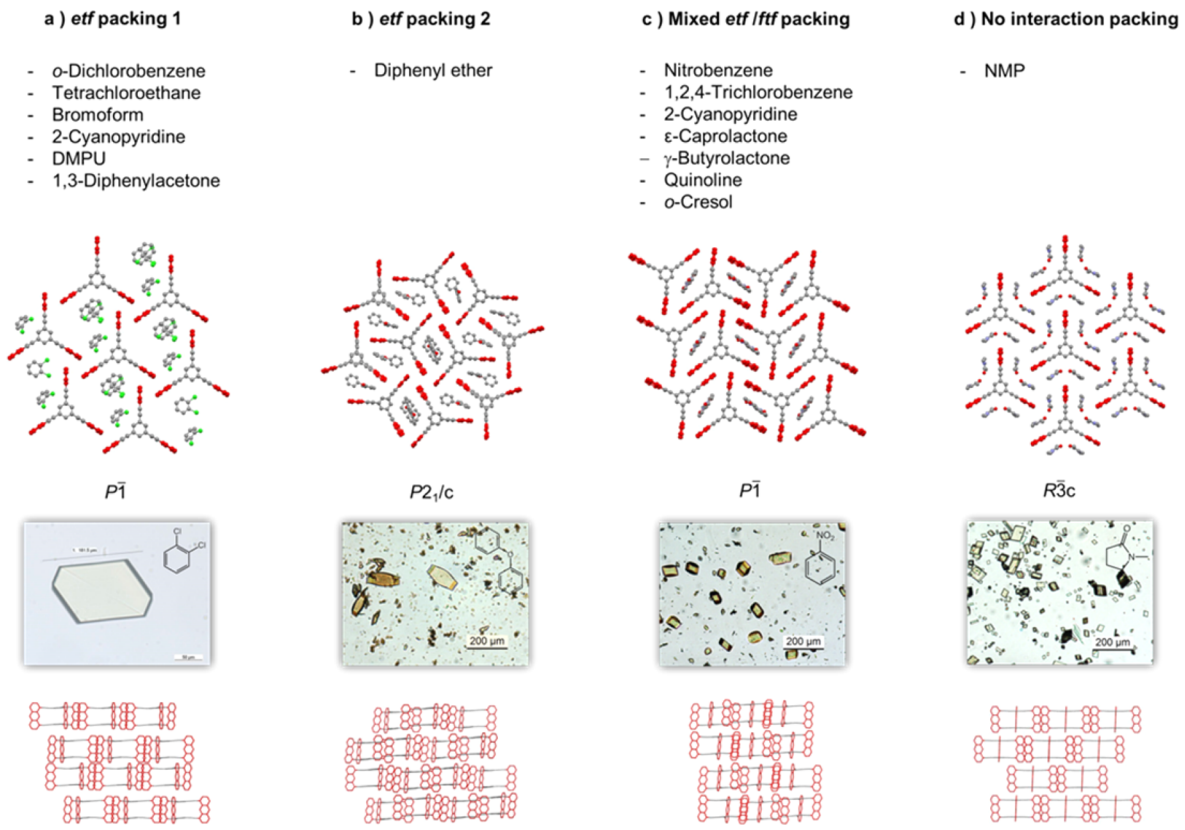

Figure 2. Four packing motifs obtained: (a) *etf* packing 1, (b) *etf* packing 2, (c) mixed *etf*/*ftf* packing, and (d) no anthracene-anthracene interaction packing. From top to bottom: solvents from which the packing can be obtained, top view of a layer in the crystal structures, space group, optical micrograph of one or more representative single crystals, layer arrangement in the crystal structure. The photoreactive anthracene units are colored in red. In the layer arrangement, solvent molecules are omitted for clarity. The micrographs do not reflect the real color. For details on the crystal structures, see the SI.

than DDQ and was therefore not investigated further. Ditriflate **7** is well soluble in most organic solvents and can be stored in the dark for months. The advantage of this novel synthetic path lies in the fact that the workups are fast and simple, not involving tedious column chromatography.

In the next stage, anthraphane precursor **9** was assembled (Scheme 1b). We opted for a one-step reaction by reacting an excess of ditriflate **7** (typically 5−6 equiv) with **8** in dioxane under standard Sonogashira conditions with $Pd(PPh_3)_4$ and CuI, as catalyst and cocatalyst, respectively, and triethylamine as base. As expected, compound **9** precipitates during the reaction, but we were pleased to see that once collected by filtration this greenish solid was already pure according to NMR. Minor inorganic impurities were removed by filtering the crude product over Celite with chloroform, resulting in the pure precursor as a bright yellow solid in yields up to 60%. Precursor **9** was crystallized from tetrachloroethane and the structure clarified by SC-XRD (see the SI). It is noted that when working with relatively large amounts of **9** (above 1 g), due to its poor solubility large amounts of solvent have to be used for the filtration over Celite and some material can get lost in this procedure. Attempts to further optimize the precursor synthesis were performed and are described in the SI.

The anthraphane monomer **3** is then prepared by reacting **9** with an equimolar amount of **8**, using $Pd(PPh_3)_4$ as catalyst. To minimize side reactions in this complex sequence of intermolecular and intramolecular couplings, copper-free Sonogashira and high dilution (1−2 mM) conditions are employed. This affords the target cyclophane **3** as a pale yellow solid in rather impressive yields ranging from 28 to 40%. Compound **3** was characterized by ^{1}H NMR spectroscopy and high-resolution mass spectrometry, but its low solubility prevented analysis by ^{13}C NMR spectroscopy. However, the proposed structure for anthraphane was unambiguously confirmed by SC-XRD analysis, due to its tendency to readily form single crystals from a variety of solvents. The solution UV/vis and fluorescence spectra of **3** do not show signs of intramolecular cross-talk between the anthracene units and are virtually superimposable with the spectra obtained from ditriflate **7** and precursor **9**. The melting point of compound **3** lies above its decomposition temperature, which is around 280 °C.

Crystallization of Anthraphane and Its Packing in the Single Crystal. Because of its low solubility, compound **3** can be best crystallized by slow cooling of nearly saturated solutions. A variety of high-boiling solvents were screened (for details see the Supporting Information, Table S1), and 14 solvents were chosen for crystallization (*o*-dichlorobenzene (ODCB), 1,1,2,2-tetrachloroethane (TCE), bromoform, 2-cyanopyridine, 1,3-dimethyl-3,4,5,6-tetrahydro-2(1*H*)-pyrimidinone (DMPU), 1,3-diphenylacetone, *N*-methylpyrrolidone (NMP), diphenyl ether, nitrobenzene, 1,2,4-trichlorobenzene, *ε*-caprolactone, *λ*-butyrolactone, quinolone, *o*-cresol). The obtained yellow crystals were in the size range of 100−200 *µ*m. Crystal morphology depends on the solvent and is not indicative of the internal packing: in other words, different solvents can result in identical packing but different crystal shape. The unit cells of several crystals from all crystallization

DOI: 10.1021/acs.joc.6b00209
J. Org. Chem. 2016, 81, 2572−2580

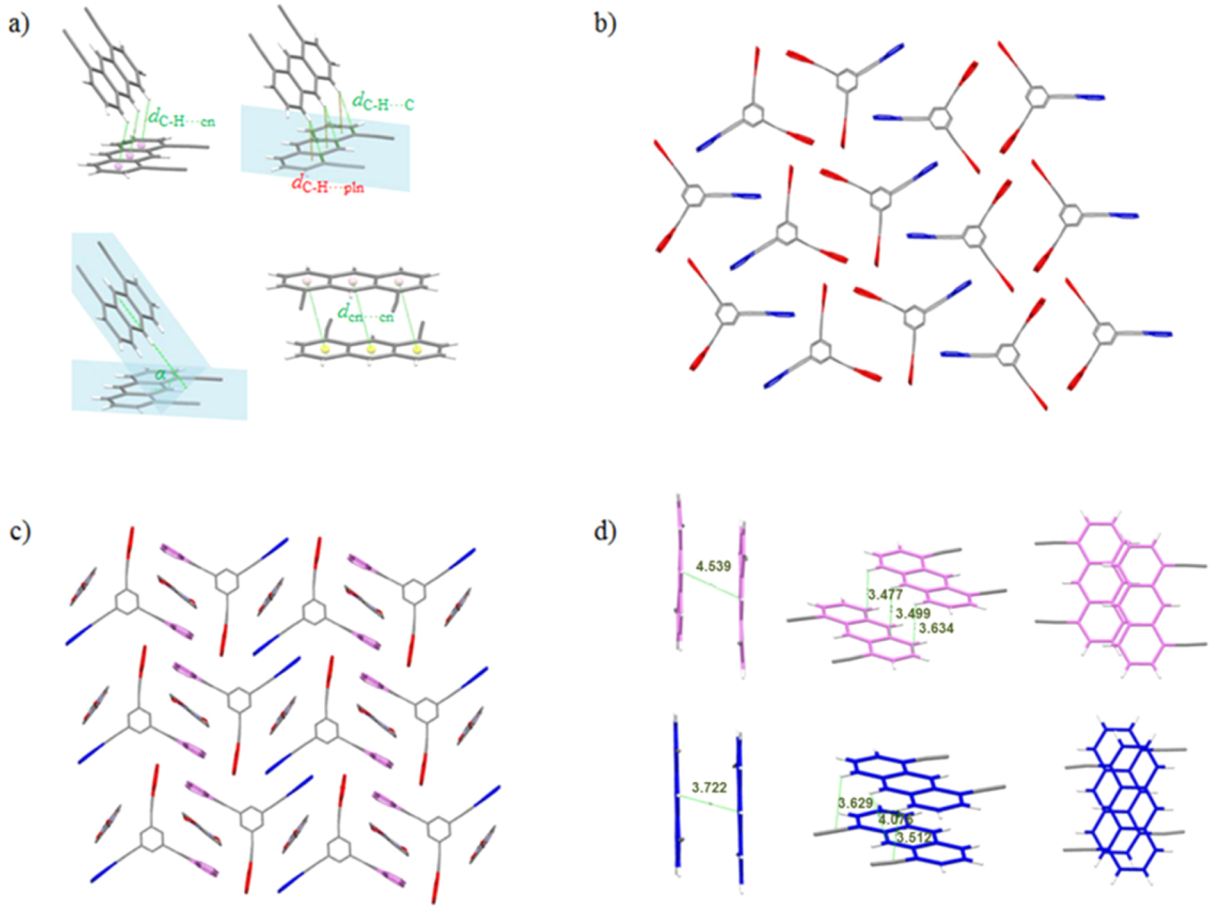

Figure 3. (a) Geometrical parameters used in this work to describe the various types of interactions. CH···π interactions: distance between H atoms and centroids of the aromatic rings $d_{C-H\cdots cn}$; distance between H atoms and anthracene plane $d_{C-H\cdots pln}$ (red), distance between H atoms and nearest C atoms $d_{C-H\cdots C}$ (green), angle between the ring planes α; $\pi\cdots\pi$ interactions: distances between rings' centroids $d_{cn\ \cdots cn}$. (b) The two types of interactions in the *etf* packing 2: the CH···π quadruplexes are displayed in red, whereas the CH···π interaction with one anthracene moiety and the acetylenic carbons is displayed in blue (solvent omitted for clarity). (c) Types of interactions in the mixed *etf*/*ftf* packing. The anthracenes involved in the CH···π quadruplexes are displayed in red and pink, whereas the anthracenes involved in the *ftf* $\pi\cdots\pi$ stacking are displayed in blue. Solvent molecules stack with the pink and blue sets of anthracenes, efficiently filling the voids. (d) Detailed view of the *ftf* $\pi\cdots\pi$ interactions involved in the mixed *etf*/*ftf* packing for the pink (top) and blue (bottom) anthracene pairs: side view of the anthracene pairs with distance from the 9 and 10 positions (left); distances between hydrogens and the closest carbon atom $d_{C-H\cdots C}$ (center); top view showing the anthracene displacement (right). Distances are in Å.

attempts were probed using SC-XRD, but not all data sets were fully solved and refined due to time-consuming sample preparation and measurements resulting from tiny samples exhibiting high mosaicity and a high degree of disorder (see SI). In some cases with similar solvent and identical cell parameters (within the standard uncertainties), only one representative structure was solved and the others were assumed to be identical in terms of packing. The four main packing motifs obtained are displayed in Figure 2, together with the solvents from which the crystals were grown. It must be noted that in all four cases anthraphane **3** crystallizes in layers. The interactions which lead to the packing motifs will be described individually in the following paragraphs on the basis of the geometric parameters displayed in Figure 3a. These parameters were chosen in accordance with the literature[25] and are differentiated according to CH···π and $\pi\cdots\pi$ interactions. For the former, the distance between the H atoms and the centroids of the aromatic rings ($d_{C-H\cdots cn}$), the distance between the H atoms and the anthracene plane ($d_{C-H\cdots pln}$), the distance between the H atoms and the nearest C atoms ($d_{C-H\cdots C}$), and the angles between the ring planes (α) are considered. For $\pi\cdots\pi$ interactions, the distance between the rings' centroids ($d_{cn\ \cdots cn}$) and the angle between the ring planes (α) are examined (for more details see the Supporting Information). The following packing scenarios were observed:

etf Packing 1. Crystals grow as clear light yellow plates from *o*-dichlorobenzene and belong to the triclinic crystal system. The packing exhibits exclusively *etf* interactions (Figure 2a) with CH···π distances $d_{C-H\cdots cn}$ ranging from 2.559(2) to 2.853(2) Å, $d_{C-H\cdots pln}$ between 2.538(2) and 2.797(2) Å, $d_{C-H\cdots C}$ between 2.763(5) and 2.948(5) Å, and angles α ranging from 54.9(2) to 68.0(2)°. These distances are shorter than the van der Waals distances (<2.97 Å[26]), which is a sign for strong CH···π interactions.[27] The voids between the monomers are filled with ODCB molecules (some of which are involved in mutual $\pi\cdots\pi$ interactions). No channels exist in the structure as the layers are arranged in a staggered fashion with no solvent molecules between layers. There are two different interlayer distances; i.e., the structure can be described as a sequence of tight bilayers with an internal layer distance of ~3.0 Å, which is separated from the next bilayer by ~4.7 Å. It is also interesting to note that the triple bonds are slightly distorted and not

DOI: 10.1021/acs.joc.6b00209
J. Org. Chem. 2016, 81, 2572−2580

coplanar with the central benzene cores, which in turn are not orthogonal to the anthracene moieties, adopting a slightly tilted conformation with angles varying from 1.4(2)° to 6.4(2)°. Interestingly, in the case of the DMPU and 1,3-diphenylacetone solvates, the layers in the structures are arranged so that channels filled with solvent molecules are formed (see Figures S18 and S21).

etf Packing 2. Crystals grow as clear light yellow convex needles from diphenyl ether and belong to the monoclinic system. The cyclophane packs in layers again, exclusively exhibiting *etf* interactions (Figure 2b). However, in this case there are two kinds of interaction motifs. In the first, two out of three anthracenes form a quadruplex of CH···π interactions. This quadruplex is marked in red in Figure 3b, with distances $d_{C-H\cdots cn}$ ranging from 2.576(1) to 3.398(1) Å, $d_{C-H\cdots pln}$ between 2.545(1) and 3.051(1) Å, and $d_{C-H\cdots C}$ between 2.762(3) and 3.281(3) Å and angles α ranging from 73.6(1) to 75.3(1)°. The other interaction involves the remaining anthracene, marked in blue in Figure 3b, and seems to be a CH···π interaction with the p-orbitals of the external acetylenic carbon atom rather than the neighboring anthracene carbon. This is supported by long distances $d_{C-H\cdots cn}$ of 3.762(2)−3.968(2) Å and short distances $d_{C-H\cdots C}$ of 2.733(5)−2.910(5) Å, which in this case correspond to the distance from the external acetylenic carbon. Compound **3** also interacts through $\pi\cdots\pi$ stacking with both sides of the aromatic unit of diphenyl ether. The voids between the cyclophanes are filled with either one or two solvent molecules, the latter being involved in a mutual $\pi\cdots\pi$ interaction with one phenyl unit, whereas the second phenyl unit interpenetrates the cyclophane layers (see Figure S26). Because of the highly distorted triple bonds the layers appear wavy, and therefore, the interlayer distance cannot be determined reliably, but it approximates to 3.4 Å. It is worth noting the distortion of the anthracene moieties with respect to the central benzene cores, two of which are tilted by 6.9(1)° and 6.4(1)° in one direction whereas one is tilted by 7.6(1)° in the other direction with respect to the ideal orthogonal geometry.

Mixed etf/ftf Packing. Crystals grow as clear yellow cylindrical plates from nitrobenzene and belong to the triclinic crystal system. Similar to the *etf* packing 2, there is a quadruplex of CH···π interactions in which two out of three anthracene moieties are involved. These are marked in red and pink in Figure 3c. However, in this case, the compound packs more densely, so that one pair of parallel anthracenes (red) interacts with the acetylene p-orbitals rather than those of the pink anthracenes, as supported by the distances $d_{C-H\cdots cn}$ of 4.031(2)−4.118(2) Å, $d_{C-H\cdots pln}$ of 2.416(5)−2.496(5) Å, and $d_{C-H\cdots C}$ of 2.701(3)−2.751(3) Å (corresponding to the external acetylene carbon) and the angle α = 69.7(1)°. In turn, the pink set of anthracenes interact with the red set through CH···π with $d_{C-H\cdots cn}$ = 2.629(2)−2.689(2) Å, $d_{C-H\cdots pln}$ = 2.623(2)−2.672(2) Å, $d_{C-H\cdots C}$ = 2.802(3)−2.906(3) Å, and α = 69.7(1)°. Another interesting consequence of this dense packing is that the pink anthracenes in the quadruplex are interacting with each other through a parallel displaced $\pi\cdots\pi$ interaction with $d_{cn\cdots cn}$ = 4.541(4)−4.591(3) Å, $d_{C-H\cdots cn}$ = 3.753(2)−3.907(2) Å, $d_{C-H\cdots pln}$ = 3.401(3)−3.609(3) Å, $d_{C-H\cdots C}$ = 3.478(4)−3.635(4) Å, and α = 0° (Figure 3d). The large $d_{cn\cdots cn}$ is similar to the distance between the 9 and 10 positions of the anthracenes (4.538(6) Å), rendering a photodimerization between this pair unlikely. The remaining blue anthracenes interact with the red set of the quadruplex according to $d_{C-H\cdots cn}$ = 3.283(2)−3.301(2) Å, $d_{C-H\cdots pln}$ = 2.852(3)−2.895(3) Å, $d_{C-H\cdots C}$ = 2.962(4)−2.981(3) Å (corresponding to the external acetylene carbon), and a small angle α = 42.9(1)°, the latter corresponding to a situation between *etf* CH···π and *ftf* $\pi\cdots\pi$. More interestingly, the blue set of anthracenes are paired with each other by a slightly displaced *ftf* $\pi\cdots\pi$ interaction, with $d_{cn\cdots cn}$ = 3.728(3)−3.740(2) Å (Figure 3d) and α = 0°. The hydrogens seemingly interact with the acetylene moieties with a $d_{C-H\cdots C}$ = 3.513(4)−3.630(4) Å. Solvent molecules efficiently fill the voids between the monomers by stacking *ftf* with the pink and blue sets of anthracene moieties. The layers are again staggered with an approximate interlayer distance of 4.9 Å. The structural skeleton is deformed, resulting in distorted triple bonds and anthracenes, one of which is tilted by 7.4(1)° in one direction. The remaining two are tilted by 1.9(1)° and 11.4(1)°, respectively, in the other direction from the ideal orthogonal geometry with respect to the central benzene core. For details on the solved crystal structures of the quinoline and *o*-cresol solvates, see the SI.

Packing with No Anthracene−Anthracene Interaction. Crystals grow as clear light yellow rhombohedra from NMP and belong to the trigonal crystal system. The cyclophanes do not interact with each other within the layers through *etf* CH···π or *ftf* $\pi\cdots\pi$ interactions (Figure 2d). In fact, every face of the anthracenes is arranged in sandwich fashion between two NMP molecules, whose methyl groups are oriented alternatively upward and downward relative to the layer plane. Additionally, every edge of an anthracene is blocked further by two NMP molecules, so that each compound is tightly surrounded by 12 NMP molecules in total. This effectively prevents all interactions between anthracenes. Examining the details of the packing (Figure S42), CH···π interactions are found between the anthracenes and one hydrogen atom of the methyl group of NMP ($d_{C-H\cdots cn}$ = 3.001(2) Å, $d_{C-H\cdots pln}$ = 2.949(2) Å, $d_{C-H\cdots C}$ = 3.073(2) Å, and α = 43.8(6)°), one hydrogen of the β-methylene ($d_{C-H\cdots cn}$ = 3.301(2) Å, $d_{C-H\cdots pln}$ = 2.872(3) Å, $d_{C-H\cdots C}$ = 2.949(4) Å, and α = 54.2(7)°), and finally, one hydrogen of the λ-methylene ($d_{C-H\cdots cn}$ = 2.629(1) Å, $d_{C-H\cdots pln}$ = 2.601(1) Å, $d_{C-H\cdots C}$ = 2.816(4) Å, and α = 64.4(5)°). Such aliphatic CH···π interactions are present in many crystal structures. Though of weak nature, they are cumulative and can dictate the arrangements in the packings.[28,29] The layers are equidistant (~3.7 Å) and are arranged in a staggered fashion without any solvent molecule located between them; hence, no channels are present in the structure. Finally, the triple bonds are only slightly distorted, with the anthracenes being almost orthogonal to the central benzene cores, showing a tilting angle of 3.1(1)°.

What can now be concluded from this variety of XRD crystal structures? Irrespective of the very different solvents employed, anthraphane always crystallized in layers, which were in no case separated from one another by embedded solvent molecules. Within the layers, the anthracene subunits are arranged virtually perpendicular to the layer's plane and the level of molecular distortions within the compounds is low, if at all existent. For compounds bearing anthracene units, the following cases of specific interactions could have been expected: *etf*, *ftf*, and mixed *etf*/*ftf*. Interestingly, while *etf* and mixed *etf*/*ftf* were actually found in several instances, all-*ftf* arrangements are absent. In addition to these specific interactions, situations in which the anthracenes do not show any particular interaction with each other can also occur. For this relatively rare case, one

DOI: 10.1021/acs.joc.6b00209
J. Org. Chem. 2016, 81, 2572−2580

example was discovered when NMP was used as solvent. From this packing, it is concluded that the interaction between the solvent NMP and compound **3** is very favorable, meaning that similar crystallization media should be avoided when trying to achieve all-*ftf* stacking.

The comparison between the *etf* packing motifs 1 and 2 shows already by visual inspection that the size of the solvent does not play a clear role: while diphenyl ether is obviously more sterically demanding than *o*-dichlorobenzene, the packing in the crystals obtained from the former is tighter than that from the latter. Moreover, 1,3-diphenylacetone, despite being sterically more demanding than both diphenyl ether and *o*-dichlorobenzene, gives rise to the same *etf* packing obtained with the latter solvent. Another interesting observation is noted in regard to the use of nitrobenzene. This strongly acceptor-substituted aromatic compound allows **3** to at least entertain one *ftf* interaction between two neighboring anthracene units. This is corroborated by 2-cyanopyridine, which has the same effect at least in one of the two polymorphs investigated. The same packing is, however, obtained also with aromatics lacking a strong acceptor character such as quinoline, *o*-cresol, and 1,2,4-trichlorobenzene. Therefore, it seems that the geometric shape of the solvents must also play a role: all solvents employed which are either flat or can easily assume a flat conformation resulted prevalently in the mixed *etf*/*ftf* packing. Thus, if *ftf* is to be favored over the other packing motifs, electron deficiency and flatness of the solvent should be considered. This conclusion should be, however, considered with great care as it is based on qualitative considerations and can only serve as an aid to the experimentalist. As is often the case, in the absence of strong directing interactions such as hydrogen bonding, halogen bonding, and coordination complexation, predicting the crystal packing of a molecule is not really possible without the aid of computational structure prediction, which is still a huge challenge.

As stated in the beginning, this work was primarily driven by the search for new monomers such as anthraphane **3**, to be used for the creation of 2D polymers through lateral topochemical polymerization. Through examination of the different XRD structures of this novel, well available cyclophane, arguments were found that could lead our research into the desired direction. These concern the role of electron deficiency and flatness in crystal packing. Analyzing the electrostatic potential surface (EPS) of cyclophane **3**, calculated with the semiempirical PM3 method,[30] we found a substantial negative charge on the faces of the anthracenes (Figure 4a). At the central aromatic ring of the anthracene, the molecular electrostatic potential (MEP) amounts to −16.3 kcal/mol. It seems reasonable to assume that it is exactly this negative potential that hampers *ftf* packing, which is therefore only partially realized when solvents showing positive electrostatic surface potentials such as nitrobenzene or 2-cyanopyridine are used. Through their attractive electrostatic interactions with the negatively polarized anthracene blades of **3**, they force some of the other anthracene blades into *ftf* arrangements, as seen in the mixed *etf*/*ftf* packing motif. While the few anthracene pairs present in the mixed *etf*/*ftf* packed crystals are likely to allow a photochemically induced dimerization, our future research will rather aim at enforcing all-*ftf* packings, e.g., by using co-crystallization of the donor compound **3** with an appropriate acceptor-substituted analogue.

Looking into the repertoire of similar compounds available to us, it seems that the substituted 1,8-diazaanthraphane derivative

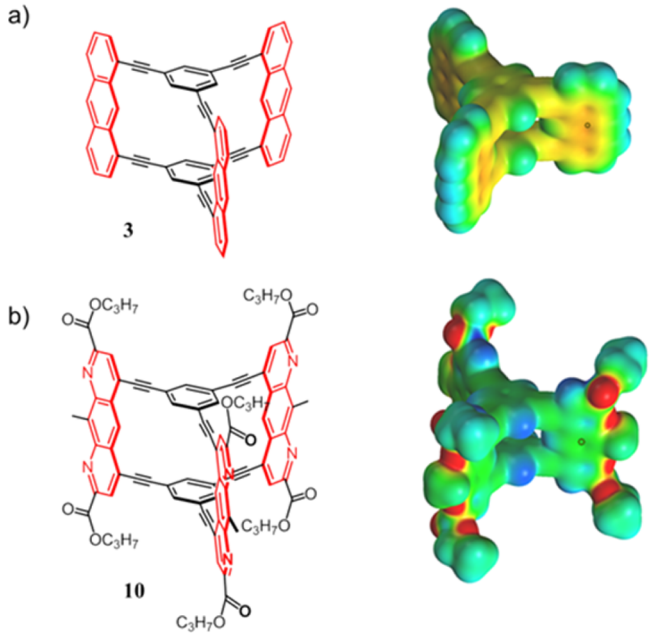

Figure 4. EPS calculated by the semiempirical PM3 method: (a) anthraphane **3**: the molecular electrostatic potential (MEP) at the marked position is −16.3 kcal/mol, classifying the compound as donor; (b) previously reported substituted 1,8-diazaanthraphane **10**; the MEP value at the marked positions is +0.7 kcal/mol, classifying the compound as a weak acceptor.

10 might be a good choice.[31] Figure 4b shows its chemical structure and calculated EPS, which exhibits a much reduced charge density at the central aromatic ring with a MEP of +0.7 kcal/mol, rendering **10** a cyclophane with a slight acceptor character and almost charge-neutral anthracene faces. These experiments will be the subject of future reports. It has to be noted that, with compound **1**, an exclusive *ftf*-packing was achieved despite the donor character of the molecule (see Figure S48). This was possible due to **1** acting as a template for the packing: together with the solvent 2-cyanopyridine and by means of parallel-displaced *ftf* interactions, a central spectating molecule forces the surrounding cyclophanes into exclusively parallel *ftf* arrangements, suitable for photodimerization. This directing template effect could not be observed in the solvates of **3**. In the case of **1**, triazine units which add additional weak interactions perpendicular to the layers are also present. Attempts to influence the interlayer interactions in **3** by using fluorinated aromatic solvents such as hexafluorobenzene were also performed, but due to the very poor solubility of anthraphane in these media, single crystals could not be grown.

CONCLUSION

We designed and synthesized a new potential monomer for the topochemical synthesis of two-dimensional polymers, "anthraphane" (**3**), a hydrocarbon cyclophane with D_{3h} symmetry bearing photoreactive anthracene units. Anthraphane was obtained in only five steps and in rather impressive yields, using the key building block anthracene-1,8-ditriflate **7**, whose synthesis was revisited and greatly simplified, allowing us to obtain gram amounts efficiently and in short times. We then crystallized anthraphane from 14 different solvents, aiming at an exclusive *ftf*-packing, suitable for topochemical photopolymerization. Although the objective was not achieved, we could show that anthraphane always crystallizes in layers. Moreover,

DOI: 10.1021/acs.joc.6b00209
J. Org. Chem. 2016, 81, 2572−2580

we proved that the solvents employed for crystallization can influence the packing within the layers, yielding different types of interaction motifs among the anthracene units of **3**. The dominant interactions encountered are all *etf* CH···π. In some solvates, however, we found partial *ftf* π···π along with *etf* CH···π interactions: this kind of packing is mostly realized with solvents that can easily obtain a flat conformation or have an acceptor character. To support our findings, we analyzed the electrostatic potential surface of anthraphane, calculated by the semiempirical PM3 method. We found strongly negative MEP values on the surface of the anthracenes, which could be the reason why the anthracenes tend to avoid *ftf* π···π in favor of *etf* CH···π and parallel-displaced π···π interactions. Although the packing for **3** that would allow photopolymerization within the single crystal has yet to be found, we believe that co-crystallization with an acceptor-substituted anthraphane such as **10** could realize an all-*ftf* packing by the means of acceptor−donor interactions. It is moreover possible that with a proper solvent, an all-*ftf* packing could be also obtained by **3** alone (as it has been shown for compound **1**); this would, however, imply continuation with a frustrating trial and error strategy.

As a final remark, we wish to point out that the synthetic strategy presented here opens the possibility for an easy desymmetrization of **3** by not reacting compound **9** with 1,3,5-triethynylbenzene (**8**) but rather a polar derivative of it. This should give rise to substituted anthraphane derivatives with amphiphilic character as would be needed in interfacial approaches to 2DPs.

EXPERIMENTAL SECTION

General Information. All reactions were carried out under nitrogen by using standard Schlenk techniques and dry solvents. DCM, dioxane, and toluene were distilled by a solvent drying system equipped with activated alumina columns under nitrogen atmosphere (H_2O content <5 ppm as determined by Karl Fischer titration). $Pd(PPh_3)_4$ catalyst was freshly prepared following the literature procedure[32] and stored in a glovebox in the dark under N_2 at room temperature. Compound **5** was prepared according to literature procedures.[24] All reagents were purchased and used without further purification. Column chromatography for purification of the products was performed by using silica gel Si60 (particle size 40−63 μm). Centrifugation was performed at 25 °C and 4000 rpm.

NMR was recorded (^{1}H, 300 MHz; ^{13}C, 75 MHz) at room temperature or 70 °C. The signal from the solvents was used as the internal standard for chemical shift (^{1}H, δ = 7.26 ppm, ^{13}C, δ = 77.16 ppm for chloroform; ^{1}H, δ = 6.00 ppm, ^{13}C, δ = 73.78 ppm for 1,1,2,2-tetrachloroethane; ^{1}H, δ = 5.33 ppm, ^{13}C, δ = 54 ppm for dichloromethane; ^{1}H, δ = 2.50 ppm, ^{13}C, δ = 39.52 ppm for dimethyl sulfoxide; ^{19}F, δ = −164.9 ppm for hexafluorobenzene). When possible, proton and carbon signal assignments were performed with the help of 2D-NMR experiments such as COSY, HSQC, and HMBC (spectra not shown).

For high-resolution mass spectrometry (HRMS) analyses, electron-spray or MALDI were used as ionization methods. For the latter, either 3-hydroxypicolinic acid (3-HPA) or *trans*-2-[3-(4-*tert*-butyl-phenyl)-2-methyl-2-propenylidene]malononitrile (DCTB) were used as the matrix.

UV/vis absorption spectra were recorded using a quartz cell with a path length of 1 cm. Emission spectra were recorded using a quartz cell with a path length of 1 cm by diluting by a factor of 30−60 (depending on the compound) the solutions employed for the UV/vis absorption measurements. Melting points are uncorrected.

SC-XRD analysis was performed on a diffractometer using a microfocus sealed-tube Cu Kα source or a graphite-monochromated sealed-tube Mo Kα radiation (λ = 0.71073 Å). Crystals were kept at 100 K during measurement.

EPS calculations were performed with Spartan software.

4a,9,9a,10-Tetrahydroanthracene-1,8-diol (5). Compound **5** was prepared following the previously reported procedure.[24] ^{1}H NMR (300 MHz, DMSO-d_6) δ/ppm: 9.39 (s, 2H), 6.97 (t, J = 7.7 Hz, 2H), 6.71 (d, J = 8.0 Hz, 2H); 6.68 (d, J = 8.2 Hz, 4H), 3.83 (s, 2H), 3.71 (s, 2H). ^{13}C NMR (75.5 MHz DMSO-d_6) δ/ppm: 154.2, 137.3, 126.2, 122.3, 118.1, 112.1, 34.9, 21.8. HRMS (FT-MALDI): m/z calcd for $C_{14}H_{13}O_2$ $[M - H]^+$: 213.0910, found 213.0909. Mp: 207−209 °C.

4a,9,9a,10-Tetrahydroanthracene-1,8-diyl Bis-(trifluoromethanesulfonate) (6). 1,8-Dihydroxy-9,10-dihydroanthracene **5** (6.00 g, 28.0 mmol, 1 equiv) was suspended in dry DCM (300 mL) and dry pyridine (7.00 mL, 84.0 mmol, 3 equiv). The suspension was cooled to 0 °C with an ice bath, and triflic anhydride (12 mL, 70.0 mmol, 2.5 equiv) was slowly added via syringe under inert atmosphere. After addition, the resulting orange solution was stirred 15 min at 0 °C followed by 2 h at room temperature. The reaction mixture was then concentrated in vacuo to approximately half of its volume, and 150 mL diethyl ether was added. The solution was washed with 10% HCl_{aq}, followed by a saturated $NaHCO_3$ solution and finally a saturated NaCl solution. The organic phase was then dried over $MgSO_4$ and concentrated to dryness. The brown residue was dissolved in boiling hexane, treated with activated charcoal, and stirred for 20 min. Hot filtration followed by concentration of the filtrate afforded **6** as a yellow oil that crystallized upon standing (12.8 g, 26.7 mmol, 96%). ^{1}H NMR (300 MHz, CD_2Cl_2) δ/ppm: 7.40 (dd, J = 7.5 Hz, 1.9 Hz, 2H); 7.36 (t, J = 7.5 Hz, 2H); 7.25 (dd, J = 7.5 Hz, 1.9 Hz, 2H); 4.11 (m, 4H). ^{19}F NMR (282.5 MHz, CD_2Cl_2) δ/ppm: −76.17. ^{13}C NMR (75.5 MHz, CD_2Cl_2) δ/ppm: 147.5, 139.6, 128.5, 128.0, 127.8, 119.9, 119.1 (q, J_{CF} = 320.1 Hz), 36.0, 24.0. HRMS (FT-MALDI): m/z calcd for $C_{16}H_{10}F_6NaO_6S_2$ $[M - Na]^+$ 498.9715, found 498.9714. Mp: 76−78 °C.

Anthracene-1,8-diyl Bis(trifluoromethanesulfonate) (7). Di-triflate **6** (8.70 g, 18.2 mmol, 1 equiv) was dissolved in dry dioxane (100 mL). DDQ (5.37 g, 23.6 mmol, 1.3 equiv) was added in one portion, and the resulting suspension was refluxed at 125 °C for 5 h (conversion monitored by ^{1}H NMR) under inert atmosphere. The red reaction mixture was cooled to room temperature and then filtered to remove the hydroquinone. The solid was washed with DCM, and the combined filtrates were concentrated to dryness. The residue was then eluted through a short silica plug (15 cm) with 20% DCM in hexane (elution followed by UV lamp at 366 nm, product appears as a blue band). Concentration of the eluate afforded pure **7** as pearly white needles (8.02 g, 16.9 mmol, 93%). ^{1}H NMR (300 MHz, $CDCl_3$) δ/ppm: 8.90 (s, 1H), 8.61 (s, 1H), 8.07 (d, J = 7.8 Hz, 2H); 7.62−7.50 (m, 4H). ^{19}F NMR (282.5 MHz, $CDCl_3$) δ/ppm: −76.36. ^{13}C NMR (75.5 MHz, $CDCl_3$) δ/ppm: 145.7, 133.1, 128.9, 127.9, 125.6, 125.4, 118.9 (q, J_{CF} = 320.3 Hz), 118.4, 114.1. HRMS (FT-MALDI): m/z calcd for $C_{16}H_8F_6O_6S_2$ $[M]^+$ 473.9661, found 473.9661. Mp: 111 °C.

(Benzene-1,3,5-triyltris(ethyne-2,1-diyl))tris(anthracene-8,1-diyl) Tris(trifluoromethanesulfonate) (9). An excess amount of ditriflate **7** (2.00 g, 4.22 mmol, 5 equiv) was placed under inert atmosphere in a 20 mL dry Schlenk tube along with 1,3,5-triethynylbenzene (**8**) (126 mg, 0.84 mmol, 1 equiv), $Pd(PPh_3)_4$ (49 mg, 0.04 mmol, 0.05 equiv), and CuI (8 mg, 0.04 mmol, 0.05 equiv). In a separate Schlenk tube, a solution of dry dioxane (8 mL) and triethylamine (0.47 mL, 3.37 mmol, 4 equiv) was degassed three times by freeze−pump−thaw cycles. The degassed solution was transferred via syringe into the reactant's vessel, and the obtained reaction mixture was stirred in the dark at 70 °C for 36 h, during which time a greenish solid formed. After cooling, the reaction mixture was filtered, and the obtained greenish solid was washed with 30 mL of dioxane and 30 mL of MeOH. The crude product was then suspended in warm chloroform and filtered over a pad of Celite to obtain a bright yellow solution. The Celite was then rinsed with copious amounts of chloroform in order to extract more product. The filtrate was concentrated to obtain **9** as a bright yellow solid (0.57 g, 0.51 mmol, 60%), which can be recrystallized from tetrachloroethane if needed. To recover the excess of starting material, the filtered reaction mixture is concentrated to dryness and the residue subjected to flash chromatography with 20% DCM in hexane as eluent (0.71 g, 1.50

DOI: 10.1021/acs.joc.6b00209
J. Org. Chem. 2016, 81, 2572−2580

mmol, 89%). ^{1}H NMR (300 MHz, CD_2Cl_4) δ/ppm: 9.36 (s, 3H), 8.61 (s, 3H), 8.19 (s, 3H), 8.16−8.08 (m, 6H), 7.98 (d, J = 7.1 Hz, 3H), 7.63 (dd, J = 8.6 Hz, 7.0 Hz, 3H), 7.58−7.50 (m, 6H). ^{13}C NMR (75.5 MHz, CD_2Cl_4) δ/ppm: 145.8, 134.5, 132.6, 131.8, 131.61, 131.57, 129.0, 128.6, 127.5, 126.0, 125.0, 124.3, 124.0, 121.3, 118.9, 118.7 (q, J_{CF} = 321.0 Hz), 117.3, 94.0, 88.0. ^{19}F NMR (282.5 MHz, CD_2Cl_4) δ/ppm: −76.65. HRMS (FT-MALDI): m/z calcd for $C_{57}H_{27}F_9O_9S_3$ $[M]^+$ 1122.0668, found 1122.0673. Mp: decomposes above 270 °C.

Anthraphane (3). Precursor **9** (0.50 g, 0.44 mmol, 1.00 equiv) was suspended in 300 mL of dry toluene (1.48 mM) with 1,3,5-triethynylbenzene **8** (66.9 mg, 0.44 mmol, 1.00 equiv) and dry triethylamine (12.0 mL, 89.0 mmol, 200 equiv). The reaction mixture was degassed by cooling to −80 °C with an acetone−dry ice bath and then performing five cycles of vacuum (10 min) and nitrogen backfilling. $Pd(PPh_3)_4$ (103 mg, 0.09 mmol, 0.20 equiv) was added with N_2 counter-flow, and the suspension was degassed twice again and backfilled with argon after the last cycle. After being warmed to room temperature, the reaction mixture was put in a preheated bath at 80 °C and stirred in the dark under argon for 7 days. After being cooled to room temperature, the reaction mixture was filtered: the filtrate was kept for further workup and the obtained brownish solid was washed with 50 mL of MeOH. It was then suspended in hot chloroform and filtered through a Celite pad to obtain a yellowish solution. The Celite pad was washed with additional warm chloroform to extract as much crude product as possible, and then the solution was concentrated to dryness. The filtrate obtained from the original reaction mixture was concentrated to dryness, and the solid residue was washed with MeOH and separated by centrifugation. The washings and centrifugations were repeated until the methanolic phase became colorless. The obtained yellowish solid was combined with the solid obtained from the Celite filtration and recrystallized from boiling tetrachloroethane to obtain pure **3** as a pale yellow crystalline solid (148 mg, 0.18 mmol, 40%). ^{1}H NMR (300 MHz, CD_2Cl_4) δ/ppm: 9.54 (s, 3H), 8.53 (s, 3H), 8.09 (d, J = 8.6 Hz, 6H), 7.86−7.78 (m, 12H), 7.53 (dd, J = 8.6 Hz, 6.9 Hz, 6H). HRMS (FT-MALDI): m/z calcd for $C_{66}H_{30}$ $[M]^+$ 822.2342, found 822.2344. Due to solubility problems, a resolved ^{13}C NMR spectrum could not be measured. Mp: decomposes above 280 °C.

■ ASSOCIATED CONTENT

Supporting Information

The Supporting Information is available free of charge on the ACS Publications website at DOI: 10.1021/acs.joc.6b00209.

^{1}H and ^{13}C NMR spectra of all compounds; UV−vis absorption and emission spectra; crystallographic data and details on the crystal packings and crystallization procedures, including optical micrographs of the single crystals; EPS calculations (PDF)

X-ray crystallographic data for compounds **3.1**−**3.8** and **9** (ZIP)

■ AUTHOR INFORMATION

Corresponding Author

*E-mail: marcosendymion@gmail.com.

Notes

The authors declare no competing financial interest.

■ ACKNOWLEDGMENTS

We thank Dr. Junji Sakamoto (Osaka University) for his input into the design of the cyclophane and Prof. A. Dieter Schlüter (Laboratory of Polymer Chemistry, ETH Zürich) for valuable scientific input and help with the writing process of this paper. We thank Michael Solar of the Small Molecule Crystallography Center (SMoCC, ETH Zürich) for single-crystal X-ray measurements; Dr. Kirill Feldman and Prof. Paul Smith (Laboratory of Polymer Technology, ETH Zürich) for access to the optical microscopy equipment; Rolf Häfliger (Laboratory of Organic Chemistry, ETH Zürich) for high-resolution mass spectrometry measurements; and Prof. B. T. King (UNR) and Prof. G. Wegner (MPI-P) for helpful discussions. Finally, we thank Prof. Wolfgang Kinzelbach (ETH Zürich) for his support with this publication. This work was supported by the ETH Zürich, Switzerland (Grant No. ETH-26 10-2).

■ REFERENCES

(1) Sakamoto, J.; van Heijst, J.; Lukin, O.; Schlüter, A. D. *Angew. Chem., Int. Ed.* **2009**, *48*, 1030−1069.

(2) Colson, J. W.; Dichtel, W. R. *Nat. Chem.* **2013**, *5*, 453−465.

(3) Payamyar, P.; Kaja, K.; Ruiz-Vargas, C.; Stemmer, A.; Murray, D. J.; Johnson, C.; King, B. T.; Schiffmann, F.; Vande Vondele, J.; Renn, A.; Götzinger, S.; Ceroni, P.; Schütz, A.; Lee, L.-T.; Zheng, Z.; Sakamoto, J.; Schlüter, A. D. *Adv. Mater.* **2014**, *26*, 2052−2058.

(4) Chen, Y.; Li, M.; Payamyar, P.; Zheng, Z.; Sakamoto, J.; Schlüter, A. D. *ACS Macro Lett.* **2014**, *3*, 153−158.

(5) Payamyar, P.; Servalli, M.; Hungerland, T.; Schütz, A.; Zheng, Z.; Borgschulte, A.; Schlüter, A. D. *Macromol. Rapid Commun.* **2015**, *36*, 151−158.

(6) Kissel, P.; Erni, R.; Schweizer, W. B.; Rossell, M. D.; King, B. T.; Bauer, T.; Götzinger, S.; Schlüter, A. D.; Sakamoto, J. *Nat. Chem.* **2012**, *4*, 287−291.

(7) Bhola, R.; Payamyar, P.; Murray, D. J.; Kumar, B.; Teator, A. J.; Schmidt, M. U.; Hammer, S. M.; Saha, A.; Sakamoto, J.; Schlüter, A. D.; King, B. T. *J. Am. Chem. Soc.* **2013**, *135*, 14134−14141.

(8) Kissel, P.; Murray, D. J.; Wulftange, W. J.; Catalano, V. J.; King, B. T. *Nat. Chem.* **2014**, *6*, 774−778.

(9) Kory, M. J.; Wörle, M.; Weber, T.; Payamyar, P.; van de Poll, S.; Dshemuchadse, J.; Trapp, N.; Schlüter, A. D. *Nat. Chem.* **2014**, *6*, 779−784.

(10) Murray, D. J.; Patterson, D. D.; Payamyar, P.; Bhola, R.; Song, W.; Lackinger, M.; Schlüter, A. D.; King, B. T. *J. Am. Chem. Soc.* **2015**, *137*, 3450−3453.

(11) Bouas-Laurent, H.; Castellan, A.; Desvergne, J. P.; Lapouyade, R. *Chem. Soc. Rev.* **2000**, *29*, 43−55.

(12) Bouas-Laurent, H.; Castellan, A.; Desvergne, J. P.; Lapouyade, R. *Chem. Soc. Rev.* **2001**, *30*, 248−263.

(13) Schmidt, G. M. J. *Solid State Photochemistry*; Verlag Chemie: Weinheim, 1976. For cases of successful topochemical photoreactions above the Schmidt distance, see: Ramamurthy, V. *Tetrahedron* **1986**, *42*, 5753−5839.

(14) Desiraju, G. R.; Vittal, J. J.; Ramanan, A. *Crystal Engineering. A Textbook*; World Scientific Publishing: Singapore, 2011.

(15) Desiraju, G. R. *Crystal Engineering. The Design of Organic Solids*; Elsevier Scientific Publisher: Amsterdam, 1989.

(16) Gleiter, R., Hopf, H., Eds. *Modern Cyclophane Chemistry*; Wiley−VCH: Weinheim, 2004; DOI: 10.1002/3527603964.

(17) Grimme, S. *Angew. Chem., Int. Ed.* **2008**, *47*, 3430−3434.

(18) Salonen, L. M.; Ellermann, M.; Diederich, F. *Angew. Chem., Int. Ed.* **2011**, *50*, 4808−4842.

(19) Wheeler, S. E. *Acc. Chem. Res.* **2013**, *46*, 1029−1038 and references cited therein.

(20) Pérez-Trujillo, M.; Maestre, I.; Jaime, C.; Alvarez-Larena, A.; Piniella, J. F.; Virgili, A. *Tetrahedron: Asymmetry* **2005**, *16*, 3084−3093.

(21) Goichi, M.; Segawa, K.; Suzuki, S.; Toyota, S. *Synthesis* **2005**, *13*, 2116−2118.

(22) Chinchilla, R.; Nájera, C. *Chem. Rev.* **2007**, *107*, 874−922.

(23) Kissel, P.; Weibel, F.; Federer, L.; Sakamoto, J.; Schlüter, A. D. *Synlett* **2008**, *2008*, 1793−1796.

(24) Kory, M. J.; Bergeler, M.; Reiher, M.; Schlüter, A. D. *Chem. - Eur. J.* **2014**, *20*, 6934−6938.

(25) Suezawa, H.; Ishihara, S.; Umezawa, Y.; Tsuboyama, S.; Nishio, M. *Eur. J. Org. Chem.* **2004**, *2004*, 4816−4822.

(26) Van der Waals radii according to Alvarez, S. *Dalton. Trans.* **2013**, *42*, 8617−8636.10.1039/c3dt50599e

DOI: 10.1021/acs.joc.6b00209
J. Org. Chem. 2016, 81, 2572−2580

(27) Umezawa, Y.; Tsuboyama, S.; Honda, K.; Uzawa, J.; Nishio, M. *Bull. Chem. Soc. Jpn.* **1998**, *71*, 1207−1213.
(28) Nishio, M. *CrystEngComm* **2004**, *6*, 130−158.
(29) Desiraju, G. R.; Steiner, T. *The Weak Hydrogen Bond in Structural Chemistry and Biology*; Oxford University Press, 1999.
(30) Klärner, F.-G.; Panitzky, J.; Preda, D.; Scott, L. T. *J. Mol. Model.* **2000**, *6*, 318−327. Semiempirical methods such as PM3 are well suited to represent the electrostatic surface potential of planar aromatic rings. DFT calculations were also carried out on smaller fragments of the cyclophanes, and they agree with the PM3 calculations. For details, see the SI..
(31) Servalli, M.; Gyr, L.; Sakamoto, J.; Schlüter, A. D. *Eur. J. Org. Chem.* **2015**, *2015*, 4519−4523.
(32) Coulson, D. R. *Inorg. Synth.* **1971**, *13*, 121.

DOI: 10.1021/acs.joc.6b00209
J. Org. Chem. 2016, 81, 2572−2580